Title	α -cluster excited states in [32]S
Author(s)	Yoshida, Yuta; Kanada-En'Yo, Yoshiko; Kobayashi, Fumiharu
Citation	Progress of Theoretical and Experimental Physics (2016), 2016
Issue Date	2016-04-15
URL	http://hdl.handle.net/2433/217684
Right	© The Author(s) 2016. Published by Oxford University Press on behalf of the Physical Society of Japan. This is an Open Access article distributed under the terms of the Creative Commons Attribution License (http://creativecommons.org/licenses/by/4.0/), which permits unrestricted reuse, distribution, and reproduction in any medium, provided the original work is properly cited.
Type	Journal Article
Textversion	publisher

PTEP

Prog. Theor. Exp. Phys. **2016**, 043D01 (22 pages)
DOI: 10.1093/ptep/ptw016

α-cluster excited states in ^{32}S

Yuta Yoshida[1,*], Yoshiko Kanada-En'yo[2], and Fumiharu Kobayashi[3]

[1]*Yukawa Institute for Theoretical Physics, Kyoto University, Kyoto 606-8502, Japan*
[2]*Department of Physics, Kyoto University, Kyoto 606-8502, Japan*
[3]*Department of Physics, Niigata University, Niigata 950-2181, Japan*
[*]E-mail: yyuta@yukawa.kyoto-u.ac.jp

Received September 24, 2015; Revised January 27, 2016; Accepted February 2, 2016; Published April 15, 2016

α-cluster excited states in ^{32}S are investigated with an extended $^{28}\mathrm{Si}+\alpha$ cluster model, in which the ^{28}Si core deformation and rotation and the α-cluster breaking are incorporated. In the generator coordinate method calculation with the extended $^{28}\mathrm{Si}+\alpha$ cluster model, the α-cluster excited states are obtained near the $^{28}\mathrm{Si}+\alpha$ threshold energy. The ^{28}Si core deformation and rotation effects, and also the α-clusters breaking in the $^{28}\mathrm{Si}+\alpha$ system, are discussed. It is found that the rotation of the oblately deformed ^{28}Si core has a significant effect on the α-cluster excited states whereas the α-cluster breaking has only a minor effect.

Subject Index D11

1. Introduction

Cluster structure is one of the important aspects in nuclear systems, in particular in light nuclei. α-cluster excited states with a spatially developed α cluster around a core nucleus have been known in $Z = N$ nuclei [1–8], and also in unstable nuclei [9–27]. Typical examples of α-cluster excited states in $Z = N$ nuclei are the $^{16}\mathrm{O}+\alpha$ cluster states in ^{20}Ne and $^{12}\mathrm{C}+\alpha$ cluster states in ^{16}O [28–35]. α-cluster excited states are also suggested in the heavier mass nuclei such as ^{44}Ti and ^{40}Ca [36–51].

Candidates for α-cluster excited states in ^{32}S were reported in the $^{28}\mathrm{Si}(^{6}\mathrm{Li}, \mathrm{d})^{32}\mathrm{S}$ (α transfer) reaction by Tanabe et al. [52] in the 1980s. A couple of states observed in the 10–15 MeV region may correspond to α-cluster excited states. Recently, in experiments on the $^{28}\mathrm{Si}+\alpha$ elastic-scattering reaction, Lönnroth et al. observed many resonances above the $^{28}\mathrm{Si}+\alpha$ threshold energy, and interpreted them as fragmentation of an α-cluster excited band starting from the bandhead energy $E_x = 10.9 \pm 0.5$ MeV, a few MeV higher than the $^{28}\mathrm{Si}+\alpha$ threshold [53]. Another experiment to investigate α-cluster excited states in ^{32}S is the inelastic scatterings on ^{32}S by Itoh et al. [54]. They observed excited states near the $^{28}\mathrm{Si}+\alpha$ threshold energy that are considered to be candidates for α-cluster excited bands with bandhead energies $E_x = 6.6$ and 7.9 MeV. To understand the α-cluster excited states in ^{32}S, theoretical studies are now required.

In the history of theoretical studies of cluster structures in the p-shell and sd-shell regions, multi-α models using the Brink–Bloch α-cluster wave functions [55] have been applied to $Z = N =$ even nuclei. With the multi-α models, systematic calculations of three-dimensional α-cluster configurations were performed from ^{16}O to ^{44}Ti [56]. For ^{28}Si, the 7α-cluster model was used to discuss the shape coexistence of the oblate and prolate states [57]. The multi-α model was also used for ^{20}Ne to take into account the ^{16}O core structure change in $^{16}\mathrm{O}+\alpha$ cluster states in ^{20}Ne [58].

However, in these studies with the multi-α models, the constituent α clusters are assumed to be the ideal $0s$-closed configuration, and therefore the contribution of the spin–orbit interaction is completely omitted even though it is significant in mid-shell nuclei. In other words, α clusters in nuclei should be more or less broken from the ideal configuration to gain the spin–orbit interaction. To take into account the α-cluster breaking and the contribution of the spin–orbit interaction, an extension of cluster models has been done in the study of the ^{16}O+α cluster states in ^{20}Ne [59]. Cluster structures in sd-shell nuclei were also investigated by antisymmetrized molecular dynamics (AMD) [5–7], in which the existence of clusters is not assumed but the formation and breaking of cluster structures are automatically described in the model. In the AMD calculation for ^{28}Si, the oblately deformed state with a 7α-like configuration was obtained for the ^{28}Si ground state consistently with the 7α-cluster model calculation [57]; however, it was shown that the oblate ground state is different from the ideal 7α configuration but it contains significant cluster breaking because of the spin–orbit interaction [60]. In the systematic studies with AMD by Taniguchi et al., α-cluster excited states were suggested in various sd-shell nuclei [61,62]. In these studies, the existence of clusters is not assumed *a priori*, but core deformation and α-cluster breaking are taken into account in the AMD framework. However, rotation of the core in the α-cluster excited states is not sufficiently considered.

Our aim in this paper is to theoretically investigate the α-cluster excited states in ^{32}S. The question to be answered is whether the α-cluster band appears near the $^{28}\mathrm{Si}+\alpha$ threshold energy. If this is the case, we are going to predict its properties such as the bandhead energy, the level spacing (the rotational constant), and the α-decay width. We also intend to clarify the core deformation and rotation effects as well as the α-cluster breaking effect in the α-cluster excited states. In α-cluster excited states in the sd-shell region, core deformation may occur, and the rotation of the deformed core could play an important role. Moreover, an α cluster at the nuclear surface can be dissociated because of the spin–orbit potential. To incorporate core deformation and rotation as well as α-cluster breaking, we construct a new extended cluster model for the $^{28}\mathrm{Si}+\alpha$ system by extending the conventional cluster model, which relies on the inert cluster assumption. We apply the method and investigate the properties of α-cluster excited states in ^{32}S.

The contents of this paper are as follows. In Sect. 2, we explain the formulation of the extended $^{28}\mathrm{Si}+\alpha$-cluster model. We show the calculated results in Sect. 3, and discuss the ^{28}Si core structure and the α-cluster breaking effect in the α-cluster excited states in ^{32}S in Sect. 4. Finally, a summary and an outlook are given in Sect. 5.

2. Framework

To investigate α-cluster excited states in ^{32}S, we construct the extended cluster model for the $^{28}\mathrm{Si}+\alpha$ system to take into account the ^{28}Si core deformation and rotation, and α-cluster breaking. In this section, we first explain the Brink–Bloch α-cluster model (a conventional cluster model), and then we describe the formulation of the extended $^{28}\mathrm{Si}+\alpha$-cluster model.

2.1. Brink–Bloch α-cluster model

In the Brink–Bloch α-cluster model [63], a $Z=N=2n$ nucleus is composed of $n\alpha$ clusters. Each α cluster is described by the $(0s)^4$ harmonic oscillator (h.o.) configuration localized around a certain position. The total $n\alpha$-cluster wave function $\Phi_{n\alpha}$ of the $A=4n$-body system is written by the

following antisymmetrized single-particle wave functions:

$$\Phi_{n\alpha}(\mathbf{R}_1, \ldots, \mathbf{R}_n) = \mathcal{A}[\Phi_\alpha(\mathbf{R}_1) \cdots \Phi_\alpha(\mathbf{R}_n)], \tag{1}$$

$$\Phi_\alpha(\mathbf{R}_i) = \varphi_{\uparrow p}(\mathbf{R}_i)\varphi_{\downarrow p}(\mathbf{R}_i)\varphi_{\uparrow n}(\mathbf{R}_i)\varphi_{\downarrow n}(\mathbf{R}_i), \tag{2}$$

$$\varphi_\sigma(\mathbf{R}_i) = \left(\frac{2\nu}{\pi}\right)^{\frac{3}{4}} \exp\left[-\nu(\mathbf{r} - \mathbf{R}_i)^2\right] \chi_\sigma \tau_\sigma, \tag{3}$$

where $\mathcal{A}$ is the antisymmetrizing operator for all nucleons, $\mathbf{R}_i$ is the center of the ith α-cluster ($i = 1, \ldots, n$), χ_σ and τ_σ are the spin and isospin parts of the single-particle wave function, respectively, and ν is the width parameter.

2.2. *Extended cluster model for α-cluster breaking*

To describe α-cluster breaking due to the spin–orbit potential from a core, we apply the method proposed by Itagaki et al. [59]. In this method, α-cluster breaking is incorporated by adding a spin-dependent imaginary part to the Gaussian centers of the single-particle wave functions so as to gain the spin–orbit potential:

$$\Phi_{\alpha'}(\mathbf{R}, \lambda_\alpha) = \mathcal{A}\left[\varphi_{\uparrow p}(\mathbf{Z}_1)\varphi_{\downarrow p}(\mathbf{Z}_2)\varphi_{\uparrow n}(\mathbf{Z}_3)\varphi_{\downarrow n}(\mathbf{Z}_4)\right], \tag{4}$$

$$\mathbf{Z}_j = \mathbf{R} + i\lambda_\alpha \frac{(\mathbf{e}_{\mathrm{spin},j}) \times (\hat{\mathbf{R}})}{\sqrt{\nu}}, \tag{5}$$

where the parameter λ_α represents the degree of the α-cluster breaking, and $\mathbf{e}_{\mathrm{spin},j}$ is the unit vector oriented to the intrinsic spin direction of the jth nucleon ($j = 1, \ldots, 4$). If λ_α is zero, this model becomes the conventional (Brink–Bloch) cluster model and describes the intrinsic spin-saturated state, where the expectation value of the spin–orbit potential vanishes. When λ_α is positive, spin-up and spin-down nucleons in the α cluster obtain finite momenta with opposite directions so as to gain the spin–orbit potential.

2.3. *Extended cluster model for* ^{28}Si *core*

To describe the ^{28}Si core structure, we adopt an extended 7α-cluster model where the parameter Λ_c for the cluster breaking is incorporated to take into account the spin–orbit interaction effect. The present extended 7α-cluster model is based on the study of ^{28}Si with the Brink–Bloch 7α-cluster model [57] and that with the AMD method [60]. Bauhoff et al. used the 7α-cluster model with a pentagon configuration [57], and succeeded in describing the oblate ground state and the $K^\pi = 5^-$ rotational band with the D_{5h} symmetry of a pentagon configuration. The 7α-cluster model wave function $\Phi_{7\alpha}$ forms a pentagon configuration as shown in Fig. 1(a), and is described as

$$\Phi_{7\alpha}(d_1, d_2) = \mathcal{A}\left[\Phi_\alpha\left(\frac{1}{2}d_1\mathbf{e}_z\right)\Phi_\alpha\left(-\frac{1}{2}d_1\mathbf{e}_z\right)\prod_{k=1}^{5}\hat{R}_z\left(\frac{2\pi}{5}k\right)\Phi_\alpha(d_2\mathbf{e}_x)\right], \tag{6}$$

where $\hat{R}_z$ is the rotation operator around the z-axis, and d_1 and d_2 are the distance parameters for 7α cluster positions.

The pentagon configuration of the 7α-cluster structure of ^{28}Si has also been supported by the AMD calculation where α clusters are not assumed *a priori* [60]. Differently from the Bauhoff's 7α-cluster model, the ^{28}Si wave function obtained by AMD for the ground state is not the ideal 7α-cluster wave function without the cluster breaking, but is a 28-body wave function with a pentagon configuration of 7α clusters with cluster breaking.

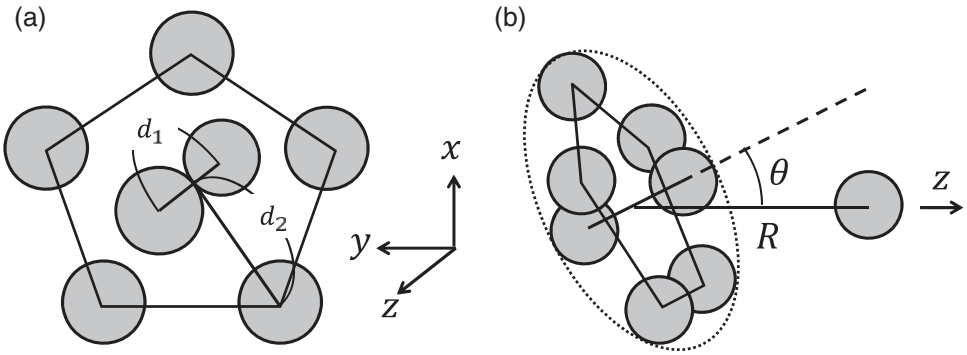

Fig. 1. Schematic figures for spatial configurations of Gaussian centers. (a) The 7α-cluster configuration with a pentagon shape for the ^{28}Si core. (b) The configuration for the present $^{28}\mathrm{Si} + \alpha$ cluster model.

Based on the AMD result for ^{28}Si, we construct an extended 7α-cluster model for the ^{28}Si core by respecting the symmetry for the $2\pi/5$ rotation as follows:

$$\Phi_{^{28}\mathrm{Si}}(d_1, d_2, \Lambda_c) = \mathcal{A}\left[\Phi_\alpha\left(\frac{1}{2}d_1\mathbf{e}_z\right)\Phi_\alpha\left(-\frac{1}{2}d_1\mathbf{e}_z\right)\sum_{k=1}^{5}\hat{R}_z\left(\frac{2\pi}{5}k\right)\Phi_{\alpha'}(d_2\mathbf{e}_x, \Lambda_c)\right], \quad (7)$$

$$\Phi_{\alpha'}(d_2\mathbf{e}_x, \Lambda_c) = \mathcal{A}\big[\varphi_{\uparrow_y p}(d_2\mathbf{e}_x + id_2\Lambda_c\mathbf{e}_z)\varphi_{\downarrow_y p}(d_2\mathbf{e}_x - id_2\Lambda_c\mathbf{e}_z) \times \varphi_{\uparrow_y n}(d_2\mathbf{e}_x + id_2\Lambda_c\mathbf{e}_z)\varphi_{\downarrow_y n}(d_2\mathbf{e}_x - id_2\Lambda_c\mathbf{e}_z)\big]. \quad (8)$$

Here, $\Phi_{\alpha'}(d_2\mathbf{e}_x, \Lambda_c)$ represents the wave function for a broken α cluster, where $\uparrow_y$ and $\downarrow_y$ are the intrinsic spin of the y direction, and nucleon momenta take the z direction. Λ_c is the parameter for the cluster breaking in the 7α-cluster model for the ^{28}Si core, and is called the 7α-cluster breaking parameter in this paper. In the case of the $d_1 \to 0$ and $d_2 \to 0$ limit, this extended 7α-cluster model wave function $\Phi_{^{28}\mathrm{Si}}(d_1 \to 0, d_2 \to 0, \Lambda_c)$ describes the $0d_{5/2}$ sub-shell closed configuration of the jj-coupling shell model at $\Lambda_c = 1$ and the oblately deformed state at $\Lambda_c = 0$. Note that 5α clusters in the ^{28}Si core are broken α clusters written by the previously mentioned method for the α-cluster breaking proposed by Itagaki et al. The concept of the present model for the ^{28}Si core is similar to that of an extended 3α cluster model for ^{12}C proposed by Suhara et al. [64].

In the present calculation, the parameters, d_1 and d_2 for the positions of 7α-clusters are fixed to be the optimized values ($d_1 = 0.20$ fm, $d_2 = 0.27$ fm) that give the minimum energy of ^{28}Si in the 7α-cluster model without cluster breaking ($\Lambda_c = 0$). Hereafter, we define the ^{28}Si wave function with fixed d_1 and d_2 values as $\Phi_{^{28}\mathrm{Si}}(\Lambda_c) \equiv \Phi_{^{28}\mathrm{Si}}(d_1 = 0.20\,\mathrm{fm}, d_2 = 0.27\,\mathrm{fm}, \Lambda_c)$, parameterized by Λ_c.

2.4. *Extended cluster model for the* $^{28}\mathrm{Si} + \alpha$ *system*

We construct the extended ^{28}Si+α-cluster model to take into account the ^{28}Si core deformation and rotation, and the α-cluster breaking. We set the ^{28}Si core and the α cluster at the inter-cluster distance R, and perform the generator coordinate method (GCM) [65,66] by treating R as the generator coordinate. The α cluster is parameterized by the α-cluster breaking parameter λ_α, whereas the ^{28}Si core is specified by the 7α-cluster breaking parameter Λ_c, which changes the ^{28}Si core deformation from the oblate state to the spherical one. In addition to these parameters, R, λ_α, and Λ_c, we consider the angle parameter θ to specify the orientation of the oblately deformed ^{28}Si core. We set

the α cluster on the z-axis and define θ for the rotation of the ^{28}Si core as shown in Fig. 1(b). When $\theta = 0^\circ$, the symmetric axis of the ^{28}Si core corresponds to the z axis.

Then, the ^{28}Si+α wave function of the extended ^{28}Si+α-cluster model is written as

$$\Phi_{^{28}\mathrm{Si}+\alpha}(R, \theta, \lambda_\alpha, \Lambda_c) = \mathcal{A}\left[\Phi_{\alpha'}\left(\tfrac{7}{8}R\mathbf{e}_z, \lambda_\alpha\right)\Phi_{^{28}\mathrm{Si}}\left(-\tfrac{1}{8}R\mathbf{e}_z, \theta, \Lambda_c\right)\right], \tag{9}$$

$$\Phi_{^{28}\mathrm{Si}}(\mathbf{R}, \theta, \Lambda_c) = \hat{T}(\mathbf{R})\hat{R}_y(\theta)\Phi_{^{28}\mathrm{Si}}(\Lambda_c), \tag{10}$$

where $\hat{T}(\mathbf{R})$ is the translation operator and $\hat{R}_y(\theta)$ is the rotation operator around the y-axis. $\Phi_{^{28}\mathrm{Si}}(\mathbf{R}, \theta, \Lambda_c)$ expresses the extended 7α-cluster model $\Phi_{^{28}\mathrm{Si}}(\Lambda_c)$ rotated by the angle θ and shifted by $\mathbf{R}$. In the extended ^{28}Si+α-cluster model, the width parameter is chosen to be $\nu = 0.16\,\mathrm{fm}^{-2}$ so as to reproduce the ^{28}Si radius with the sub-shell closed configuration.

2.5. *Parity and total angular momentum projection*

We project the ^{28}Si+α wave function $\Phi_{^{28}\mathrm{Si}+\alpha}(R, \theta, \lambda_\alpha, \Lambda_c)$ to the parity and total angular momentum eigenstate,

$$\Phi^{J^\pm}_{^{28}\mathrm{Si}+\alpha}(R, \theta, \lambda_\alpha, \Lambda_c) = \hat{P}^J_{MK}\hat{P}^\pm\Phi_{^{28}\mathrm{Si}+\alpha}(R, \theta, \lambda_\alpha, \Lambda_c), \tag{11}$$

where $\hat{P}^\pm$ and $\hat{P}^J_{MK}$ are the parity and the total angular momentum projection operators, respectively. In the present paper, we only take the $K = 0$ component and omit K-mixing for simplicity.

2.6. *Generator coordinate method (GCM)*

To calculate the energy levels of α-cluster states in ^{32}S, we perform the GCM calculation by superposing the $^{28}\mathrm{Si} + \alpha$ wave function,

$$\Psi^{J^\pm_n}_{^{28}\mathrm{Si}+\alpha} = \sum_i c_i^{(n)}\Phi^{J^\pm}_{^{28}\mathrm{Si}+\alpha}(R_i, \theta_i, \lambda_\alpha = 0, \Lambda_{ci}), \tag{12}$$

where the coefficients $c_i^{(n)}$ are determined by diagonalizing the norm and Hamiltonian matrices. For the inter-cluster distance R, we superpose the wave functions with $R = 1, 2, \ldots, 10$ fm. For the 7α-cluster breaking parameter Λ_c of the ^{28}Si core, we take two points, $\Lambda_c = 0.38$ and 0.80, which correspond to oblate and spherical local minimum states of the intrinsic energy of the ^{28}Si core, as described later. For the rotation angle θ of the ^{28}Si core, we take $\theta = 0^\circ, 30^\circ, 60^\circ, 90^\circ$ for the oblate core ($\Lambda_c = 0.38$) and take $\theta = 0^\circ$ for the spherical core ($\Lambda_c = 0.80$).

In the present GCM calculation, we omit the α-cluster breaking and fix $\lambda_\alpha = 0$. More details of the choice of the parameters are described later. We call the calculation with the full diagonalization of the norm and Hamiltonian matrices in the above-mentioned basis wave functions with the parameters $(R_i, \theta_i, \Lambda_{ci})$ the "full-GCM" calculation.

2.7. *Frozen core GCM*

In the asymptotic region at a large inter-cluster distance R, the ^{28}Si core in the lowest $^{28}\mathrm{Si} + \alpha$ channel should be the ground state of an isolate ^{28}Si: $^{28}\mathrm{Si}(0^+_{\mathrm{g.s.}})$. We also perform the GCM calculation for the $^{28}\mathrm{Si}(0^+_{\mathrm{g.s.}}) + \alpha$ within the frozen core approximation and compare the result with the previously explained full GCM calculation. We call this calculation the "frozen core GCM." In the present work, we express the frozen core wave function by a linear combination of the projected $^{28}\mathrm{Si}(0^+_{\mathrm{g.s.}}) + \alpha$ wave functions as follows.

Let us first consider the adiabatic picture where the ^{28}Si configuration is optimized at each state of a given inter-cluster distance R. We define the R-fixed $^{28}\mathrm{Si}+\alpha$ wave function as

$$\Phi^{J^\pm}_{^{28}\mathrm{Si}'+\alpha}(R) = \hat{P}^J_{MK}\hat{P}^\pm\mathcal{A}\left[\Phi_\alpha\left(\frac{7}{8}R,\lambda_\alpha\right)\sum_k a_k(R)\Phi_{^{28}\mathrm{Si}}\left(-\frac{1}{8}R,\theta_k,\Lambda_{ck}\right)\right], \tag{13}$$

where parameters $(\theta_k,\Lambda_{ck}) = (0^\circ,0.38),(30^\circ,0.38),(60^\circ,0.38),(90^\circ,0.38)$, and $(0^\circ,0.80)$ are taken. Here, the coefficients $a_k(R)$ are determined by diagonalizing the norm and Hamiltonian matrices for each inter-cluster distance R. By taking a large enough inter-cluster distance R_{max}, we determine the coefficients $a_k(R_{\mathrm{max}})$ in the asymptotic region, which approximately express the ground state configuration of the ^{28}Si core. We take $R_{\mathrm{max}} = 10$ fm in this paper.

Next, using the coefficients $a_k(R_{\mathrm{max}})$ determined at R_{max}, we define the R-fixed $^{28}\mathrm{Si}(0^+_{\mathrm{g.s.}})+\alpha$ wave function with the frozen core (the R-fixed frozen core wave function):

$$\Phi^{J^\pm}_{^{28}\mathrm{Si}(0^+_{g.s.})+\alpha}(R) = \hat{P}^J_{MK}\hat{P}^\pm\mathcal{A}\left[\Phi_\alpha\left(\frac{7}{8}R,\lambda_\alpha\right)\sum_k a_k(R_{\mathrm{max}})\Phi_{^{28}\mathrm{Si}}\left(-\frac{1}{8}R,\theta_k,\Lambda_{ck}\right)\right]. \tag{14}$$

Then, we perform the frozen core GCM calculation, that is, the GCM calculation of the $^{28}\mathrm{Si}(0^+_{\mathrm{g.s.}})+\alpha$ cluster model, by superposing the $^{28}\mathrm{Si}(0^+_{\mathrm{g.s.}})+\alpha$ wave functions with different distances:

$$\Psi^{J^\pm_n}_{^{28}\mathrm{Si}(0^+_{\mathrm{g.s.}})+\alpha} = \sum_i b^{(n)}_i \Phi^{J^\pm}_{^{28}\mathrm{Si}(0^+_{\mathrm{g.s.}})+\alpha}(R_i), \tag{15}$$

where the coefficients $b^{(n)}_k$ are determined by diagonalizing the norm and Hamiltonian matrices.

2.8. $^{28}\mathrm{Si}(0^+_{\mathrm{g.s.}})+\alpha$ amplitudes in ^{32}S wave functions

In order to analyze the α-cluster motion in ^{32}S states obtained by the full-GCM and the frozen core GCM calculations, we calculate the overlap between the ^{32}S wave functions with the R-fixed $^{28}\mathrm{Si}(0^+_{\mathrm{g.s.}})+\alpha$ wave function to evaluate the α-cluster component at R:

$$f^{J^\pm_n}_{^{28}\mathrm{Si}+\alpha}(R) = \left|\left\langle\Phi^{J^\pm}_{^{28}\mathrm{Si}(0^+_{\mathrm{g.s.}})+\alpha}(R)\middle|\Psi^{J^\pm_n}_{^{28}\mathrm{Si}+\alpha}\right\rangle\right|, \tag{16}$$

$$f^{J^\pm_n}_{^{28}\mathrm{Si}(0^+_{\mathrm{g.s.}})+\alpha}(R) = \left|\left\langle\Phi^{J^\pm}_{^{28}\mathrm{Si}(0^+_{\mathrm{g.s.}})+\alpha}(R)\middle|\Psi^{J^\pm_n}_{^{28}\mathrm{Si}(0^+_{\mathrm{g.s.}})+\alpha}\right\rangle\right|. \tag{17}$$

2.9. Hamiltonian

The Hamiltonian operator ($\hat{H}$) is

$$\hat{H} = \hat{T} + \hat{V}_{\mathrm{nuclear}} + \hat{V}_{\mathrm{coulomb}} - \hat{T}_G, \tag{18}$$

$$\hat{V}_{\mathrm{nuclear}} = \hat{V}_c + \hat{V}_{LS}, \tag{19}$$

where $\hat{T}$ is the kinetic energy and $\hat{T}_G$ is the energy of the center-of-mass motion. As for the effective nuclear force $\hat{V}_{\mathrm{nuclear}}$, Volkov No.2 [67] is adopted as the central force $\hat{V}_c$ and the two-range Gaussian form of the spin–orbit term in the G3SR force [68] is used as the spin–orbit force $\hat{V}_{LS}$.

The form of Volkov No.2 is given as

$$\hat{V}_c = \sum_{i<j}^{A}\sum_{k=1}^{2} v_k \exp\left[-\left(\frac{\hat{\mathbf{r}}_{ij}}{a_k}\right)^2\right](W - MP_{\sigma\tau}), \tag{20}$$

where $v_1 = -60.65$ MeV, $v_2 = 61.14$ MeV, $a_1 = 1.80$ fm, and $a_2 = 1.01$ fm. M is the Majorana parameter, which is adjustable. In the present paper, we use $M = 0.67$. With the Volkov force,

reproductions of the binding energy of ^{32}S and the α-separation energy (^{28}Si + α threshold) are not satisfactory. We also use other M values of the Volkov force to discuss the interaction dependence of the calculated results.

The spin–orbit force is given as

$$\hat{V}_{LS} = \sum_{i<j}^{A}\sum_{k=1}^{2} u_k \exp\left[-\left(\frac{\hat{\mathbf{r}}_{ij}}{b_k}\right)^2\right] P(^3O)\,\hat{\mathbf{L}}\cdot\hat{\mathbf{S}}, \tag{21}$$

$$(^3\mathrm{O}) = \frac{1+P_\sigma}{2}\frac{1+P_\tau}{2}, \tag{22}$$

where $b_1 = 0.477$ fm, $b_2 = 0.600$ fm, and $P(^3\mathrm{O})$ is the triplet-odd projection operator. We use the strength parameters $u_1 = 2000$ MeV and $u_2 = -2000$ MeV, which are the same as those used in Ref. [59] for the $^{16}\mathrm{O} + \alpha$ system. The two-body Coulomb force in $\hat{V}_{\mathrm{coulomb}}$ is approximated by seven Gaussians.

3. Results

3.1. ^{28}Si *core structure in* ^{28}Si+α *system*

To discuss the effects of the 7α-cluster breaking in the ^{28}Si core because of the spin–orbit interaction, we show, in Fig. 2, the Λ_c dependence of the energy of an isolate ^{28}Si state before and after the parity and total angular momentum projection,

$$E_{^{28}\mathrm{Si}}(\Lambda_c) = \frac{\left\langle \Phi_{^{28}\mathrm{Si}}(\Lambda_c)|\hat{H}|\Phi_{^{28}\mathrm{Si}}(\Lambda_c)\right\rangle}{\left\langle \Phi_{^{28}\mathrm{Si}}(\Lambda_c)|\Phi_{^{28}\mathrm{Si}}(\Lambda_c)\right\rangle}, \tag{23}$$

$$E^{0^+}_{^{28}\mathrm{Si}}(\Lambda_c) = \frac{\left\langle \Phi^{0^+}_{^{28}\mathrm{Si}}(\Lambda_c)|\hat{H}|\Phi^{0^+}_{^{28}\mathrm{Si}}(\Lambda_c)\right\rangle}{\left\langle \Phi^{0^+}_{^{28}\mathrm{Si}}(\Lambda_c)|\Phi^{0^+}_{^{28}\mathrm{Si}}(\Lambda_c)\right\rangle}, \tag{24}$$

$$\Phi^{0^+}_{^{28}\mathrm{Si}}(\Lambda_c) = \hat{P}^{J=0}_{MK=0}\hat{P}^{+}\Phi_{^{28}\mathrm{Si}}(\Lambda_c). \tag{25}$$

In the $\Lambda_c = 0.3$–1.0 region, the ^{28}Si system gains much of the spin–orbit interaction energy from the 7α-cluster breaking. In the energy curve of $E_{^{28}\mathrm{Si}}$ before the parity and total angular momentum projection, there exist two energy minima at $\Lambda_c = 0.38$ and $\Lambda_c = 0.80$, though the energy almost degenerates in this region. We call these two minima of ^{28}Si the "oblate-type ($\Lambda_c = 0.38$)" and "spherical-type ($\Lambda_c = 0.80$)" states. Here, the oblate-type state is different from the $\Lambda_c = 0$ state that is the ideal state with the $(200)^4(110)^4(020)^4$ configuration in terms of the (n_x, n_y, n_z) notation of the h.o. shell-model basis in the *sd* shell. The energy of the oblate-type state at $\Lambda_c = 0.38$ is about 18 MeV lower due to the 7α-cluster breaking than that of the $\Lambda_c = 0$ state having no contribution of the spin–orbit interaction. This result supports the AMD calculation of ^{28}Si [60] and indicates that the present method of the extended 7α-cluster model is suitable to incorporate the significant energy gain of ^{28}Si with the 7α-cluster breaking in the oblately deformed ^{28}Si. In the 0^+ projected ^{28}Si energy, it is found that the oblate-type ($\Lambda_c = 0.38$) state gains further energy because of the restoration of the rotational symmetry. The present result for the ^{28}Si core indicates that the rotation of the oblately deformed state can be an important degree of freedom of the ^{28}Si core structure in the $^{28}\mathrm{Si} + \alpha$ system as well as the 7α-cluster breaking due to the spin–orbit interaction.

Next, we discuss how the ^{28}Si core structure in the $^{28}\mathrm{Si} + \alpha$ system is affected by the existence of an α cluster. The α cluster at the surface of the ^{28}Si core may affect the feature of the ^{28}Si core because

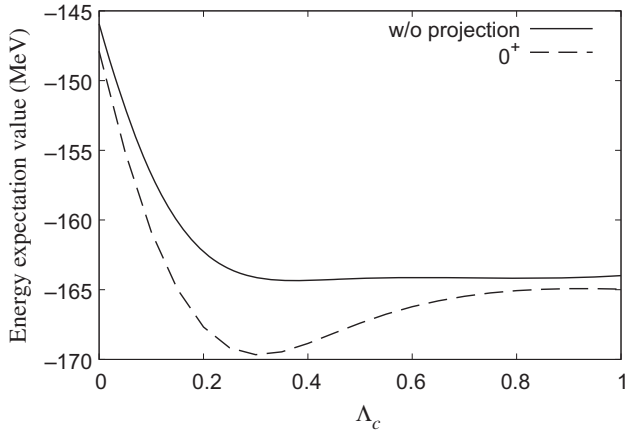

Fig. 2. The energy expectation value of the isolate ^{28}Si core. The energy $E_{^{28}\mathrm{Si}}(\Lambda_c)$ before the parity and total angular momentum projection, and the energy $E^{0^+}_{^{28}\mathrm{Si}}(\Lambda_c)$ after the projection are shown by solid and dashed lines, respectively. The width parameter is taken to be $\nu = 0.16\,\mathrm{fm}^{-2}$.

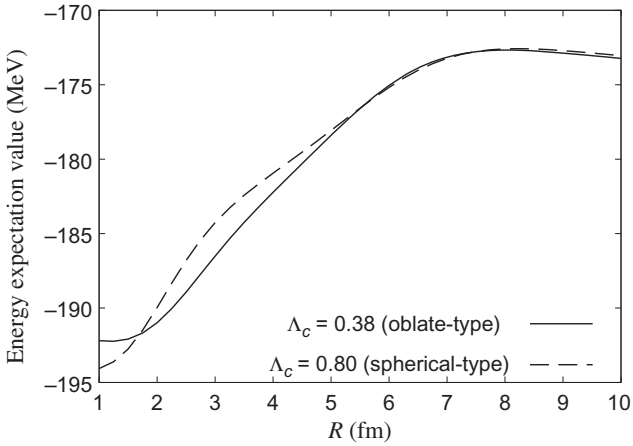

Fig. 3. Energy expectation value of $^{28}\mathrm{Si} + \alpha$ system ($E^{+}_{^{28}\mathrm{Si}+\alpha}(R, \theta = 0^\circ, \lambda_\alpha = 0, \Lambda_c)$) as a function of the inter-cluster distance R. The parameter Λ_c for the ^{28}Si core structure is fixed to be $\Lambda_c = 0.38$ (oblate type: solid) and $\Lambda_c = 0.80$ (spherical type: dashed).

of the nuclear and Coulomb interactions and also the Pauli blocking effect. To discuss features of the ^{28}Si core with an α cluster at a certain distance R from the core, we fix the parameter $\lambda_\alpha = 0$ to assume an α cluster without the breaking, and consider the 7α-breaking in the ^{28}Si core and also the orientation of the oblate-type ^{28}Si core in the $^{28}\mathrm{Si} + \alpha$ system. Namely, we analyze the energy expectation value of the parity-projected state before the total angular momentum projection,

$$E^{+}_{^{28}\mathrm{Si}+\alpha}(R, \theta, \lambda_\alpha, \Lambda_c) = \frac{\left\langle \Phi^{+}_{^{28}\mathrm{Si}+\alpha}(R, \theta, \lambda_\alpha, \Lambda_c) | \hat{H} | \Phi^{+}_{^{28}\mathrm{Si}+\alpha}(R, \theta, \lambda_\alpha, \Lambda_c) \right\rangle}{\left\langle \Phi^{+}_{^{28}\mathrm{Si}+\alpha}(R, \theta, \lambda_\alpha, \Lambda_c) | \Phi^{+}_{^{28}\mathrm{Si}+\alpha}(R, \theta, \lambda_\alpha, \Lambda_c) \right\rangle}, \tag{26}$$

$$\Phi^{+}_{^{28}\mathrm{Si}+\alpha}(R, \theta, \lambda_\alpha, \Lambda_c) = \hat{P}^{+} \Phi_{^{28}\mathrm{Si}+\alpha}(R, \theta, \lambda_\alpha, \Lambda_c), \tag{27}$$

with $\lambda_\alpha = 0$.

Figure 3 shows the $^{28}\mathrm{Si} + \alpha$ energies for the oblate-type ^{28}Si core ($\Lambda_c = 0.38$) and the spherical-type ^{28}Si core ($\Lambda_c = 0.80$) set at the orientation $\theta = 0^\circ$. The energies are plotted as functions of

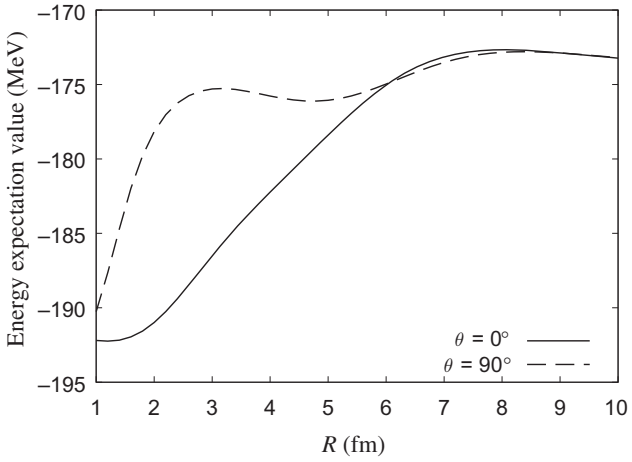

Fig. 4. Energy expectation value of $^{28}\mathrm{Si}+\alpha$ system ($E^{+}_{^{28}\mathrm{Si}+\alpha}(R,\theta,\lambda_\alpha=0,\Lambda_c=0.38)$) as a function of the inter-cluster distance R. The rotation angle θ of the oblate core is fixed to be $\theta=0^\circ$ (solid) and $\theta=90^\circ$ (dashed).

the inter-cluster distance R. It is found that, in the $R=8$ fm region, the energies of the two cases ($\Lambda_c=0.38$ and 0.80) almost degenerate as expected from the energy degeneracy in the isolate ^{28}Si. In the $2<R<5$ fm region, the energy for the oblate core is lower than that for the spherical core, indicating that, when an α cluster exists at the surface, the oblate-type ^{28}Si core is energetically favored over the spherical type because of the smaller overlap, i.e., the weaker Pauli blocking of nucleons between the α cluster and the core for the oblate core at $\theta=0^\circ$, than in the spherical core case.

To see the θ dependence of the $^{28}\mathrm{Si}+\alpha$ energy, we plot the energy expectation value $E^{+}_{^{28}\mathrm{Si}+\alpha}(R,\theta,\lambda_\alpha=0,\Lambda_c=0.38)$ of the oblate-type ^{28}Si core oriented at $\theta=0^\circ$ and 90° in Fig. 4. In the small-R region ($R<5$ fm), the $\theta=0^\circ$-oriented core is favored because of the weaker Pauli blocking than the $\theta=90^\circ$-oriented core. On the other hand, the energy does not depend on the core orientation in the large-R region, in which the rotational symmetry of the ^{28}Si core is restored. In the $6<R<8$ fm region around the barrier, the $\theta=90^\circ$-oriented core gains slightly larger potential energy than the $\theta=0^\circ$ core, but the energy difference is minor.

3.2. *α-cluster breaking*

We analyze the λ_α dependence of the energy expectation value of the $^{28}\mathrm{Si}+\alpha$ system to see the α-cluster breaking effect on the $^{28}\mathrm{Si}+\alpha$ system. Figure 5 shows the energy $E_{^{28}\mathrm{Si}+\alpha}(R,\theta=0^\circ,\lambda_\alpha,\Lambda_c=0.38)$ with the α-cluster breaking, namely, λ_α, optimized at each distance R, compared with the energy for $\lambda_\alpha=0$ without the α-cluster breaking. The energy gain by the α-cluster breaking is very small, except for the $R<3$ fm region. This result indicates that the α-cluster breaking in the $^{28}\mathrm{Si}+\alpha$ system is minor in the α-cluster excited states having large amplitudes of the α cluster at the surface region ($4<R<6$ fm). Therefore, we ignore the α-cluster breaking effect in the GCM calculation discussed in the next subsection for simplicity.

In the $R<2$ fm region, the finite λ_α gives some energy gain to the $^{28}\mathrm{Si}+\alpha$ system, but it is not appropriate to regard it as the α-cluster breaking because the α-cluster gets into in the inner region of the core and the $^{28}\mathrm{Si}+\alpha$ picture breaks down in this region. More details of the α-cluster breaking in the $^{28}\mathrm{Si}+\alpha$ system are discussed later.

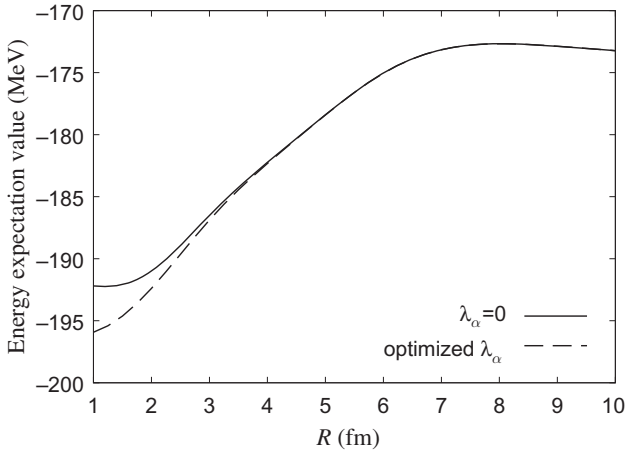

Fig. 5. Energy expectation value of $^{28}\mathrm{Si}+\alpha$ system ($E^{+}_{^{28}\mathrm{Si}+\alpha}(R, \theta=0^{\circ}, \lambda_{\alpha}, \Lambda_{c}=0.38)$) for the optimized λ_{α} as a function of the inter-cluster distance R (dashed). The energy for $\lambda_{\alpha}=0$ is also shown for comparison (solid).

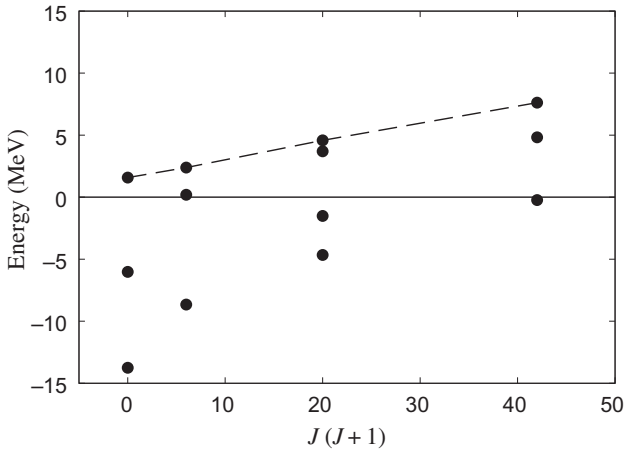

Fig. 6. The energy levels of $^{32}\mathrm{S}$ obtained by the full-GCM calculation. The energies are measured from the $^{28}\mathrm{Si}+\alpha$ threshold. The dashed line indicates the members of the α-cluster band.

3.3. GCM calculation

We superpose $^{28}\mathrm{Si}+\alpha$ wave functions and obtain the ground and excited states of $^{32}\mathrm{S}$ with the full-GCM calculation described in Sect. 2.6.

The calculated value of the $^{32}\mathrm{S}$ binding energy is 205.71 MeV, which underestimates the experimental binding energy (271.78 MeV), whereas that of the α-separation energy is 13.8 MeV, which overestimates the experimental value (6.95 MeV). We can adjust the interaction parameter M of the Volkov force to reproduce either the binding energy or the α-separation energy, but it is difficult to reproduce both data within the present two-body effective interaction. At the end of this section, we show energy levels calculated by using modified interaction parameters to see the interaction dependence of the result.

Figure 6 shows the energy levels $^{32}\mathrm{S}$ obtained by the full-GCM calculation with the default interaction parameters. Energies measured from the $^{28}\mathrm{Si}+\alpha$ threshold energy are plotted as functions of $J(J+1)$. In the energy region near the $^{28}\mathrm{Si}+\alpha$ threshold, we obtain $J^{\pm}=0^{+}, 2^{+}, 4^{+}$, and 6^{+} states having a remarkably developed α-cluster structure. We assign these states as α-cluster excited

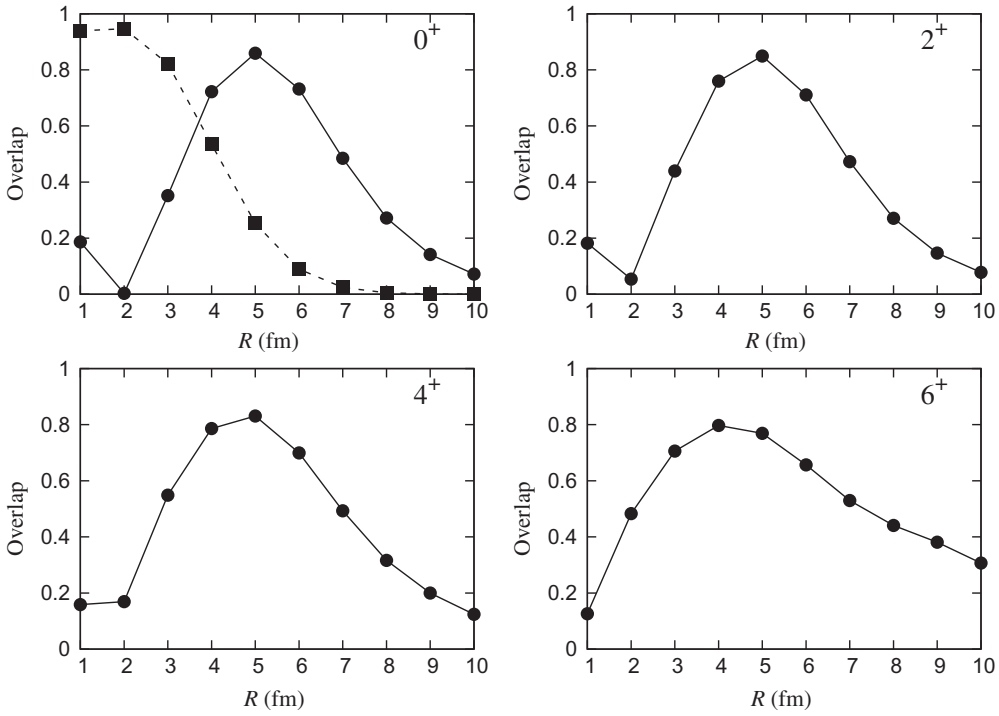

Fig. 7. The overlap $f^{J^+_n}_{^{28}\mathrm{Si}+\alpha}(R)$ for the α-cluster excited states with $J^\pm = 0^+, 2^+, 4^+$, and 6^+ (filled circles). The overlap for the ground state is also shown by filled squares in the upper left panel.

states belonging to an α-cluster band. In Fig. 6, the corresponding α-cluster excited states are shown by circles connected by dashed lines. The bandhead 0^+ state starts from $E_r = 1.58\,\mathrm{MeV}$ above the $^{28}\mathrm{Si} + \alpha$ threshold, and the rotational energy approximately follows the expression of the rigid rotor model:

$$E_{\mathrm{rot}} = \frac{\hbar^2}{2\mathcal{J}} J(J+1), \tag{28}$$

with the rotational constant $k = \hbar^2/2\mathcal{J} = 145\,\mathrm{keV}$ up to the 6^+ state. We do not obtain an α-cluster excited state with $J^\pm = 8^+$. We also obtain other excited states lower than the α-cluster excited states, but their energies change with the increase in the number of bases and we cannot obtain converged energies. This means that the present model space of the extended $^{28}\mathrm{Si} + \alpha$ cluster model is not sufficient to describe non-cluster states of $^{32}\mathrm{S}$ in the low-energy region. On the other hand, we obtain good convergence for the energies of the ground state and the α-cluster excited states with respect to the increase of the number of bases.

We show the overlap $f^{J^\pm_n}_{^{28}\mathrm{Si}+\alpha}(R)$ defined in Eq. (16) between the full-GCM wave function $\Psi^{J^\pm_n}_{^{28}\mathrm{Si}+\alpha}$ and the R-fixed frozen core wave function $\Phi^{J^\pm}_{^{28}\mathrm{Si}(0^+_{\mathrm{g.s.}})+\alpha}(R)$ for the α-cluster excited states ($J^\pm = 0^+, 2^+, 4^+, 6^+$) in Fig. 7. We also show the overlap for the ground state. The overlap $f^{J^\pm_n}_{^{28}\mathrm{Si}+\alpha}(R)$ indicates the α-cluster amplitude at R in the $L = J$ orbit around the $^{28}\mathrm{Si}$ ground state. It is found that the ground state has no developed α cluster in the large-R region. In contrast to the ground state, the α-cluster excited states show the developed α-cluster in the large-R region: the 0^+, 2^+, and 4^+ states have large amplitudes in the $R \sim 5\,\mathrm{fm}$ region, whereas the 6^+ state has a peak at $R = 4\,\mathrm{fm}$ with a long tail in the large-R region.

Table 1. The reduced α-decay widths $\theta_\alpha^2(a)$ at the channel radii $a = 6$ and $a = 7$ fm and the partial α-decay widths Γ_α for the $^{28}\mathrm{Si}(0^+_{\mathrm{g.s.}}) + \alpha$ channel in the $L = J$-wave. The results calculated with $M = 0.67$ are shown. The α-decay energies used in the calculation of Γ_α are the calculated values starting from $E_r = 1.6$ MeV, and those shifted by 2.3 MeV to adjust the bandhead energy to the experimental value $E_r = 3.9$ MeV reported in Ref. [53].

	Calculate ($M = 0.67$)					Shifted		
		$\Gamma_\alpha(a)$ (MeV)		$\theta_\alpha^2(a)$			$\Gamma_\alpha(a)$ (MeV)	
State $J^\pm$	E_r (MeV) Cal.	$a = 6$	$a = 7$	$a = 6$	$a = 7$	E_r (MeV) Shifted	$a = 6$	$a = 7$
0^+	1.6	9.9×10^{-8}	2.3×10^{-7}	0.32	0.16	3.9	0.033	0.039
2^+	2.4	2.3×10^{-5}	5.3×10^{-5}	0.30	0.16	4.7	0.060	0.068
4^+	4.6	0.0062	0.014	0.29	0.17	6.9	0.17	0.19
6^+	7.6	0.039	0.098	0.26	0.20	9.9	0.23	0.34

We estimate the α-decay widths of the α-cluster excited states using the overlap $f^{J^\pm_n}_{^{28}\mathrm{Si}+\alpha}(R)$ defined in Eq. (16) with the approximation method in Ref. [69]. Following the method in Ref. [69], the (dimensionless) reduced α width $\theta_\alpha^2(a)$ at the channel radius a is approximately evaluated by the overlap as

$$\theta_\alpha^2(a) \approx \frac{a}{3}\sqrt{\frac{\gamma}{2\pi}}\left(f^{J^\pm_n}_{^{28}\mathrm{Si}+\alpha}(a)\right)^2, \tag{29}$$

$$\gamma = \frac{A_1 A_2}{A}\nu, \tag{30}$$

where A, A_1, and A_2 are the mass numbers of ^{32}S, ^{28}Si, and the α cluster, respectively. Using $\theta_\alpha^2(a)$, we calculated the partial α-decay width Γ_α of the $^{28}\mathrm{Si}(0^+_{\mathrm{g.s.}}) + \alpha$ channel in the L-wave ($L = J$) as

$$\Gamma_\alpha = 2P_L(a)\theta_\alpha^2(a)\gamma_{\mathrm{w}}^2(a), \tag{31}$$

$$P_L(a) = \frac{ka}{F_L^2(ka) + G_L^2(ka)}, \tag{32}$$

where F_L and G_L are the regular and irregular Coulomb functions, respectively, γ_{w}^2 is the Wigner limit of the reduced α-width $\gamma_{\mathrm{w}}^2 = 3\hbar^2/2\mu a^2$, μ is the reduced mass, and $k = \sqrt{2\mu E_r}/\hbar$. The calculated $\theta_\alpha^2(a)$ and Γ_α of the α-cluster band in ^{32}S are shown in Table 1. At $a = 6$ fm, the reduced α widths are significant as $\theta_\alpha^2(a) = 0.26 \sim 0.32$ reflecting the spatially developed cluster structure in this band. For the α-decay widths, we calculate Γ_α in two cases of the bandhead energy considering the ambiguity of the predicted bandhead energy because the α-decay width is quite sensitive to the α-decay energy. In the first case, we use the energies obtained in the present calculation, in which the bandhead energy is $E_r = 1.6$ MeV. In the second case, we shift the energies by 2.3 MeV by hand to adjust the bandhead energy to the experimental value $E_r = 3.9$ MeV reported by Lönnroth et al. [53].

Let us discuss the comparison with the experimental reports of the α-cluster excited states. In the experiment of elastic $^{28}\mathrm{Si} + \alpha$ scattering, Lönnroth et al. reported the α-cluster excited band starting from the bandhead energy $E_r = 3.9 \pm 0.5$ MeV measured from the $^{28}\mathrm{Si} + \alpha$ threshold [53]. They evaluated the rotational constant $k = 122 \sim 152$ keV from the averaged energies of the fragmented states. In the experiment of α inelastic scattering on ^{32}S, Itoh et al. suggested candidates for two α-cluster excited bands at bandhead energies $E_r = -0.4$ MeV and $E_r = 0.9$ MeV with the rotational constants $k = 125$ keV and $k = 234$ keV, respectively [54]. The calculated bandhead energy

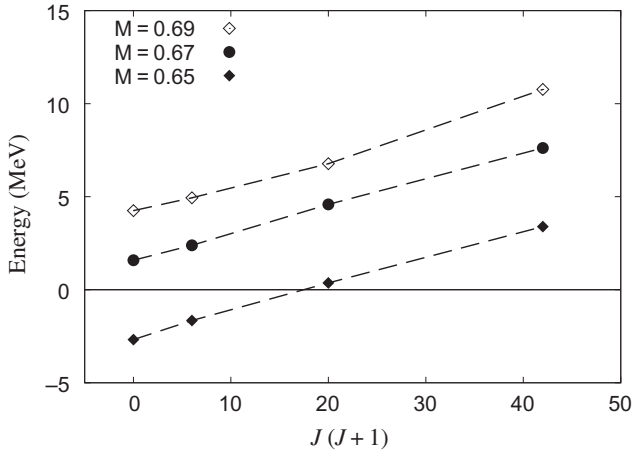

Fig. 8. The energy levels of the α-cluster band in ^{32}S obtained by the full-GCM calculation using $M = 0.69$, 0.67, and 0.65. The energies measured from the ^{28}Si + α threshold are plotted.

$E_r = 1.58$ MeV obtained with $M = 0.67$ is an intermediate value between those experimental reports. The rotational constant $k = 145$ keV in the present result is within the range of the data reported by Lönnroth et al. [53], whereas it is slightly larger than the value $k = 125$ keV for the band at $E_r = -0.4$ MeV reported by Itoh et al. Although the α-cluster excited states observed by Lönnroth et al. are fragmented, the fragmentation of the α-cluster band is not found in the present result, because the present model space may be insufficient to describe the fragmentation.

As mentioned previously, it is difficult to reproduce experimental data of both the binding energy (271.8 MeV) and the α-separation energy (6.95 MeV) of ^{32}S with the present effective interaction, and therefore we cannot quantitatively predict the energy positions of excited states. We discuss here the interaction parameter dependence of the energy position of the α-cluster excited band. We modify the Majorana parameter M in the Volkov No.2 force from $M = 0.67$ to $M = 0.69$, which reproduces the α-separation energy (6.41 MeV) but underestimates the binding energy of ^{32}S (172.2 MeV). We also use $M = 0.65$, which gives the binding energy of 239.8 MeV and α-separation energy of 21.74 MeV. In Fig. 8, we show energy levels of the α-cluster excited band obtained with $M = 0.69$, 0.67, and 0.65. The bandhead energy $E_r = 4.25$ MeV and the rotational constant $k = 149$ keV are obtained with $M = 0.69$, and $E_r = -2.68$ MeV and $k = 146$ keV are obtained with $M = 0.65$. The bandhead energy depends on the interaction parameter and ranges from $E_r = -2.68$ MeV to $E_r = 4.25$ MeV with these M values. In contrast to the strong interaction dependence of the bandhead energy, the rotational constant is not sensitive to the interaction parameter in the present calculation. Although it is difficult to quantitatively predict the bandhead energy in the present calculation, we can say that the α-cluster excited states appear near the ^{28}Si+α threshold and construct the rotational band up to the $J^\pi = 6^+$ state with the rotational constant $k = 140$–150 keV.

4. Discussion

4.1. Core rotation and shape-mixing effects

In the full-GCM calculation, we take into account the core rotation and the oblate-spherical mixing as well as the inter-cluster motion by superposing the parity and total angular momentum projected ^{28}Si+α wave functions with R, θ, and Λ_c. For the inter-cluster distance, $R = 1, 2, \ldots, 10$ fm are used. For the rotation angle of the ^{28}Si core, $\theta = 0^\circ, 30^\circ, 60^\circ, 90^\circ$ are used for the oblate core ($\Lambda_c = 0.38$), and θ is fixed to be $\theta = 0^\circ$ for the spherical core ($\Lambda_c = 0.80$). Here, we perform

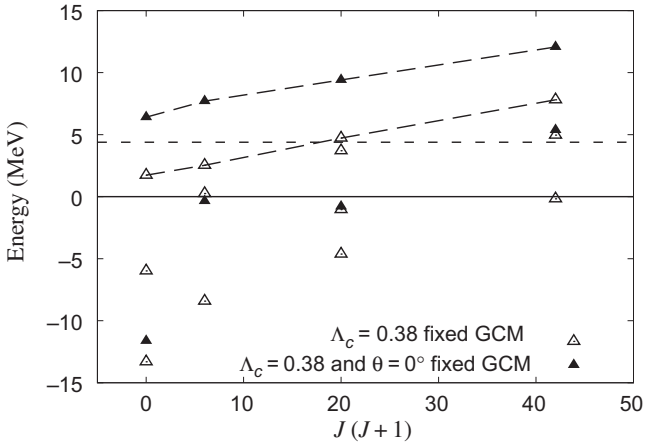

Fig. 9. The energy levels of ^{32}S obtained by the $\Lambda_c = 0.38$ and $\theta = 0^\circ$ fixed GCM calculation (filled triangle) and the $\Lambda_c = 0.38$ fixed GCM calculation (open triangle). The energies are measured from the $^{28}\mathrm{Si} + \alpha$ threshold (solid line), and the $^{28}\mathrm{Si}(\Lambda_c = 0.38) + \alpha$ threshold is plotted by the dotted line. The α-cluster bands are connected by dashed lines.

GCM calculations with reduced basis wave functions to discuss how the core rotation and the oblate-spherical mixing affect the α-cluster excited states.

We discuss the core rotation effect on the energy spectra. In Fig. 9, we compare the energy spectra obtained by the GCM calculations of the oblate core with and without the core rotation. The former is calculated by superposing ^{28}Si+α wave functions with $R = 1, \ldots, 10$ fm for the $\Lambda_c = 0.38$ core at $\theta = (0^\circ, 30^\circ, 60^\circ, 90^\circ)$, and the latter is calculated by those with $R = 1, \ldots, 10$ fm for the $\Lambda_c = 0.38$ core at the fixed angle $\theta = 0^\circ$. The mixing of the spherical core ($\Lambda_c = 0.80$) is omitted in this analysis for simplicity. As the result, the energy reduction by the core rotation is remarkable for the α-cluster excited states. The band energy is reduced by about 5 MeV, which is almost consistent with the 4.4 MeV reduction of the $^{28}\mathrm{Si}(\Lambda_c = 0.38) + \alpha$ threshold caused by the 0^+ projection of ^{28}Si. This indicates that, in the α-cluster excited states, the α cluster spatially develops and does not disturb the oblate core rotation.

In Fig. 10, we show the energy spectra obtained by the GCM calculation with full base wave functions and that without the spherical core ($\Lambda_c = 0.80$) wave functions to see the effect of the oblate-spherical mixing. The result shows that the spherical core mixing effect is minor.

4.2. Analysis in the weak coupling picture: frozen core GCM calculation

In the asymptotic region at a large inter-cluster distance R, the ^{28}Si core should be the ground state of the isolate $^{28}\mathrm{Si}(0^+_{\mathrm{g.s.}})$. As discussed previously, the α-cluster excited states contain dominantly the $^{28}\mathrm{Si}(0^+_{\mathrm{g.s.}})+\alpha$ component. Therefore, it is expected that the frozen core GCM calculation with the inert $^{28}\mathrm{Si}(0^+_{\mathrm{g.s.}})$ core assumption can be a leading-order approximation, at least for the α-cluster excited states. The frozen core GCM calculation is the extreme case of the weak coupling and it is different from the adiabatic picture of the strong coupling. In the previous section, we start from the strong coupling picture, in which the deformed ^{28}Si core is located at a fixed orientation, and then consider the rotation and shape mixing effects on the α-cluster excited states obtained by the full GCM calculation. In this section, we discuss the features of the α-cluster excited states from the weak coupling picture. Namely, we start from the frozen core $^{28}\mathrm{Si}(0^+_{\mathrm{g.s.}})+\alpha$ states, and then consider the effect of the core excitations, in particular, the rotational excitation from $^{28}\mathrm{Si}(0^+_{\mathrm{g.s.}})$. Note that the

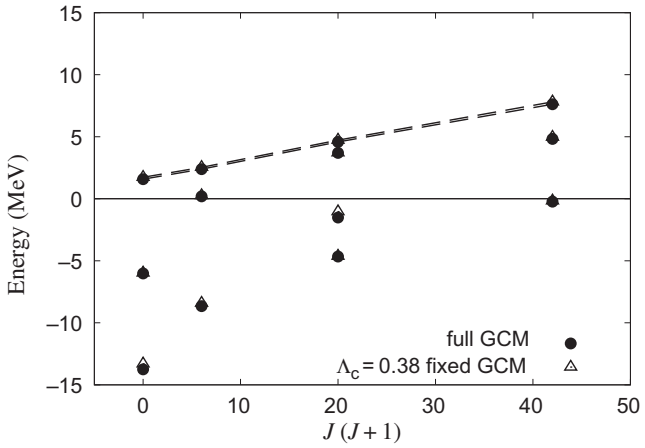

Fig. 10. The energy levels of ^{32}S obtained by the $\Lambda_c = 0.38$ fixed GCM calculation and full-GCM calculation (filled circle). The energies are measured from the $^{28}\mathrm{Si} + \alpha$ threshold (solid line). The α-cluster bands are connected by dashed lines.

core excitations taken into account in the present model are the rotational excitation such as $^{28}\mathrm{Si}(2^+)$ and also the change of the oblate-spherical mixing (shape mixing) from $^{28}\mathrm{Si}(0^+_{\mathrm{g.s.}})$.

After comparing the properties of the R-fixed $^{28}\mathrm{Si}{+}\alpha$ wave function between the optimized ^{28}Si core and the inert $^{28}\mathrm{Si}(0^+_{\mathrm{g.s.}})$ core cases, we compare the result of the frozen core GCM calculation with that of the full GCM calculation containing the rotational and shape-mixing excitations from the $^{28}\mathrm{Si}(0^+_{\mathrm{g.s.}})$ core.

For a certain inter-cluster distance R, we define the R-fixed frozen core wave function $\Phi^{J^\pm}_{^{28}\mathrm{Si}(0^+_{\mathrm{g.s.}})+\alpha}(R)$ in Eq. (14), and also the R-fixed $^{28}\mathrm{Si} + \alpha$ wave function $\Phi^{J^\pm}_{^{28}\mathrm{Si}'+\alpha}(R)$ in Eq. (13), where the ^{28}Si core wave function is optimized so as to minimize the energy expectation value of the R-fixed $^{28}\mathrm{Si} + \alpha$ wave function. Here we consider 0^+ projected wave functions. In the asymptotic region at a large inter-cluster distance R, $\Phi^{J^\pm}_{^{28}\mathrm{Si}'+\alpha}(R)$ is equal to $\Phi^{J^\pm}_{^{28}\mathrm{Si}(0^+_{\mathrm{g.s.}})+\alpha}(R)$. On the other hand $\Phi^{J^\pm}_{^{28}\mathrm{Si}'+\alpha}(R)$ may deviate from $\Phi^{J^\pm}_{^{28}\mathrm{Si}(0^+_{\mathrm{g.s.}})+\alpha}(R)$ in the short inter-cluster distance region in which the core excitation from $^{28}\mathrm{Si}(0^+_{\mathrm{g.s.}})$ occurs because of the existence of the α cluster to gain the total energy.

We plot the energy expectation values of the R-fixed frozen core wave function and the R-fixed $^{28}\mathrm{Si} + \alpha$ wave function in Fig. 11. In Fig. 12, we show the overlap between the R-fixed $^{28}\mathrm{Si} + \alpha$ wave function and the frozen core wave function,

$$f(R) = \left|\left\langle \Phi^{0^+}_{^{28}\mathrm{Si}(0^+_{\mathrm{g.s.}})+\alpha}(R) | \Phi^{0^+}_{^{28}\mathrm{Si}'+\alpha}(R) \right\rangle\right|, \tag{33}$$

which is reduced from 1 by the core excitation. It is found that the core excitation from $^{28}\mathrm{Si}(0^+_{\mathrm{g.s.}})$ occurs in the $R < 6$ fm region and it reduces the energy of the total system ^{32}S in $R \leq 5$ fm. These results indicate that the $R > 6$ fm region is understood as the ideal weak coupling regime of $^{28}\mathrm{Si}(0^+_{\mathrm{g.s.}})+\alpha$, whereas the rotational and shape-mixing excitations of the ^{28}Si core occur in the $R < 6$ fm region.

Next, we compare the frozen core GCM calculation given by Eq. (15) with the full-GCM calculation to see the core excitation effects, in particular on the α-cluster band. Figure 13 shows the energy spectra obtained by the full-GCM and the frozen core GCM calculations. The energy of the ground

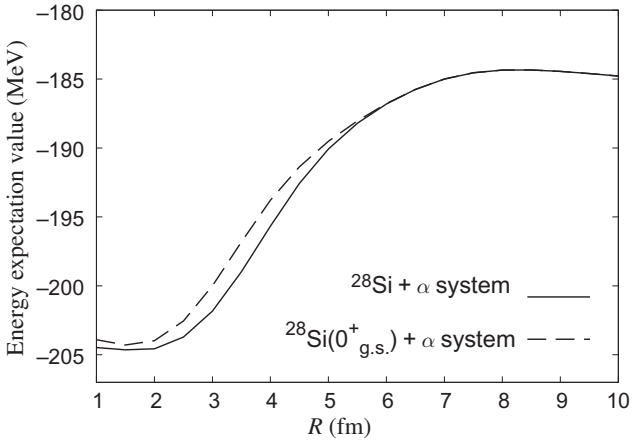

Fig. 11. Energy expectation values of the R-fixed $^{28}\mathrm{Si}+\alpha$ system and the R-fixed $^{28}\mathrm{Si}(0^+_{\mathrm{g.s.}})+\alpha$ system are plotted. The solid line is the $^{28}\mathrm{Si}+\alpha$ system and the dashed line is the $^{28}\mathrm{Si}(0^+_{\mathrm{g.s.}})+\alpha$ system.

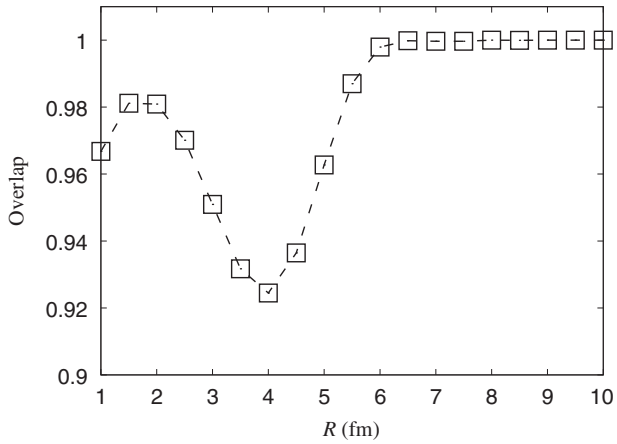

Fig. 12. The wave function overlap $f(R)$ between the R-fixed $^{28}\mathrm{Si}+\alpha$ system and the R-fixed $^{28}\mathrm{Si}(0^+_{\mathrm{g.s.}})+\alpha$ system defined in Eq. (33).

state decreases by about 1 MeV from the frozen core GCM to the full-GCM calculation. The energy of the α-cluster band also shifts down slightly because of the core excitation effect.

In Fig. 14, we compare the overlap $f^{J^\pm_n}_{^{28}\mathrm{Si}(0^+_{\mathrm{g.s.}})+\alpha}(R)$ (Eq. 17) for the frozen core GCM and $f^{J^\pm_n}_{^{28}\mathrm{Si}+\alpha}(R)$ (Eq. 16) for the full-GCM. Compared with the α-cluster amplitudes for the frozen core GCM calculation, those in the full-GCM calculation tend to be slightly suppressed in the outer region ($R \geq 5$ fm). This indicates that the α cluster is attracted toward the inner region because of the ^{28}Si core excitation such as deformation and rotation, which gives additional attraction in the $R < 5$ fm region as discussed previously. In other words, the core excitation plays a role to stabilize the α-cluster excited states.

4.3. α-cluster breaking at the nuclear surface

As mentioned in Sect. 3.2, the α-cluster breaking around the ^{28}Si core is minor in the surface region. We discuss here details of the α-cluster breaking around the ^{28}Si core in the ^{28}Si+α system in comparison with that around the ^{16}O core in the ^{16}O+α system to clarify the core dependence of the α-cluster breaking.

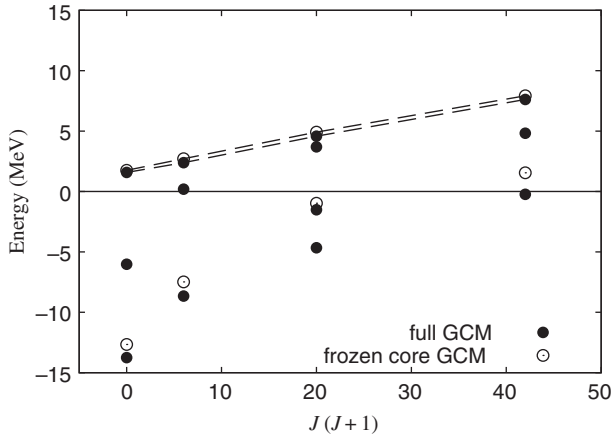

Fig. 13. The energy levels of ^{32}S obtained by the frozen core GCM calculation (open circle) and the full-GCM calculation (filled circle). The energies are measured from the $^{28}\mathrm{Si}+\alpha$ threshold (solid line). The α-cluster bands are connected by dashed lines.

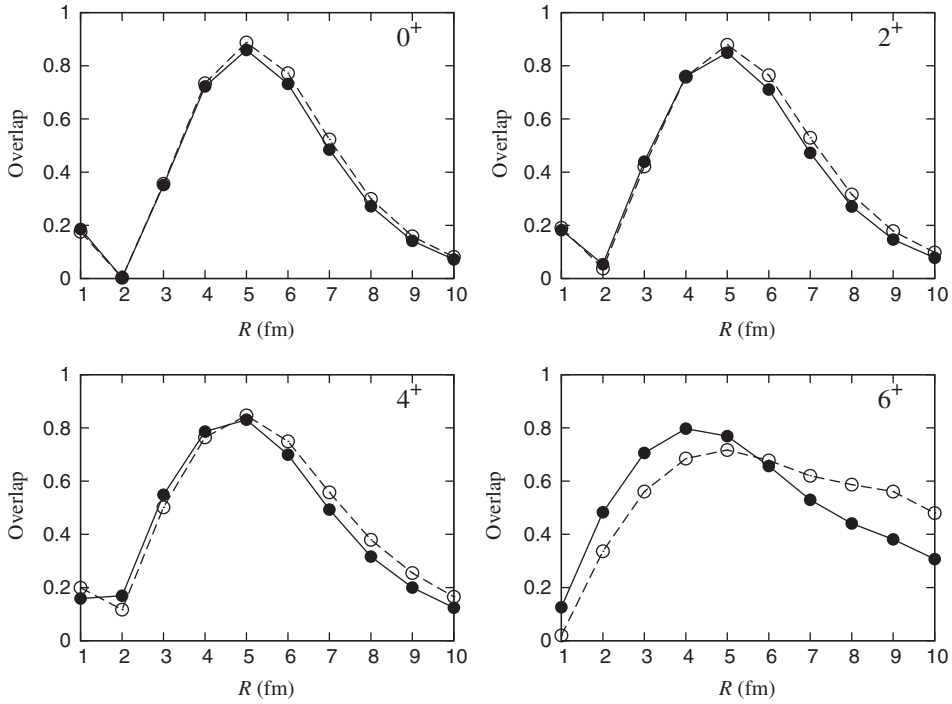

Fig. 14. The overlaps between the full-GCM wave function $\Psi^{J^\pm_n}_{^{28}\mathrm{Si}+\alpha}$ and the R-fixed frozen core wave function $\Phi^{J^\pm}_{^{28}\mathrm{Si}(0^+_{\mathrm{g.s.}})}(R)$ (filled circle), and those between the frozen core wave function $\Psi^{J^\pm_n}_{^{28}\mathrm{Si}(0^+_{\mathrm{g.s.}})+\alpha}$ and the R-fixed frozen core wave function $\Phi^{J^\pm}_{^{28}\mathrm{Si}(0^+_{\mathrm{g.s.}})}(R)$ (open circle) of the α-cluster band.

We perform a similar analysis of the α-cluster breaking for the ^{16}O+α system by using the following ^{16}O+α model wave function:

$$\Phi_{^{16}\mathrm{O}+\alpha}(R,\lambda_\alpha)=\mathcal{A}\left[\Phi_{\alpha'}\left(\tfrac{4}{5}R\mathbf{e}_z,\lambda_\alpha\right)\Phi_{^{16}\mathrm{O}}\left(-\tfrac{1}{5}R\mathbf{e}_z\right)\right], \tag{34}$$

$$\Phi_{^{16}\mathrm{O}}(\mathbf{R})=\hat{T}(\mathbf{R})\Phi_{^{16}\mathrm{O}}, \tag{35}$$

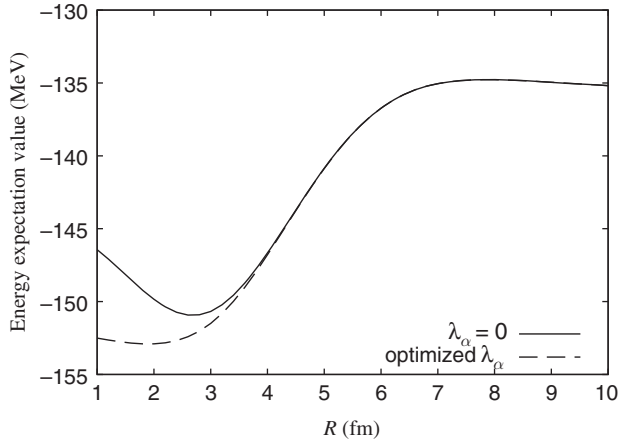

Fig. 15. Energy expectation value of the $^{16}\mathrm{O}+\alpha$ system for the optimized λ_α as a function of the inter-cluster distance R (dashed line). The energy for $\lambda_\alpha = 0$ is also shown for comparison (solid line).

where the ^{16}O core wave function $\Phi_{^{16}\mathrm{O}}$ is written by a tetrahedron formed by 4α-clusters with α–α distance 0.5 fm, which is almost equivalent to the double closed p-shell configuration. The width parameter is taken to be $\nu = 0.195\,\mathrm{fm}^{-2}$. λ_α is optimized to minimize the energy expectation value of the parity-projected $^{16}\mathrm{O}+\alpha$ wave function,

$$E^{+}_{^{16}\mathrm{O}+\alpha}(R,\lambda_\alpha) = \frac{\left\langle P^{+}\Phi_{^{16}\mathrm{O}+\alpha}(R,\lambda_\alpha)|\hat{H}|P^{+}\Phi_{^{16}\mathrm{O}+\alpha}(R,\lambda_\alpha)\right\rangle}{\left\langle P^{+}\Phi_{^{16}\mathrm{O}+\alpha}(R,\lambda_\alpha)|P^{+}\Phi_{^{16}\mathrm{O}+\alpha}(R,\lambda_\alpha)\right\rangle}. \tag{36}$$

Figure 15 shows the energy of the R-fixed ^{16}O+α wave function with the optimized λ_α (with the α-cluster breaking) and that with the fixed $\lambda_\alpha = 0$ (without the α-cluster breaking). As discussed previously, for the ^{28}Si core case, the energy reduction by the α-cluster breaking is found only in the very short distance region (see Fig. 5), whereas there is almost no energy reduction in the $R \geq 3$ fm region where the α-cluster excited states have the α-cluster amplitudes. Differently from the ^{28}Si+α system, in the $^{16}\mathrm{O}+\alpha$ system the significant energy reduction by the α-cluster breaking is found in a relatively wide R region. This energy reduction by the α-cluster breaking shifts the energy minimum position to the short distance region, and it may have a significant effect on the α-cluster structure in the ground band of ^{20}Ne, as discussed in Ref. [59]. In Fig. 16, we show the energy reduction by the α breaking, i.e., the energy difference between the optimized λ_α and the fixed $\lambda_\alpha = 0$ cases for the $^{16}\mathrm{O}+\alpha$ and $^{28}\mathrm{Si}+\alpha$ ($\Lambda_c = 0.38$) systems. We also show the energy reduction for the spherical ^{28}Si core ($\Lambda_c = 0.80$) case. It is found that the energy reduction of the ^{28}Si+α ($\Lambda_c = 0.38$) system is about half of that of the $^{16}\mathrm{O}+\alpha$ system in the $R = 2$–3 fm region, and that of the ^{28}Si+α ($\Lambda_c = 0.80$) system is quite small. Thus the α-cluster breaking gives energetically less important effects for the ^{28}Si+α system than the $^{16}\mathrm{O}+\alpha$ system.

In Fig. 17, we compare the optimized values of the α-breaking parameter λ_α for each system. In both the cases of the oblate and spherical ^{28}Si cores, the λ_α of the $^{28}\mathrm{Si}+\alpha$ system is smaller than that of the $^{16}\mathrm{O}+\alpha$ system, at least in the $R < 4$ fm region. This indicates that, compared with the $^{16}\mathrm{O}+\alpha$ system, the α-cluster breaking is relatively suppressed in $^{28}\mathrm{Si}+\alpha$, in particular for the case of the spherical-type ^{28}Si core ($\Lambda_c = 0.80$).

The α-cluster breaking at the nuclear surface is caused mainly by the spin–orbit potential from the core nucleus, and therefore it is naively expected that the α-cluster breaking is likely to occur in heavier-core systems because of the stronger core potential than light-core systems. The present result

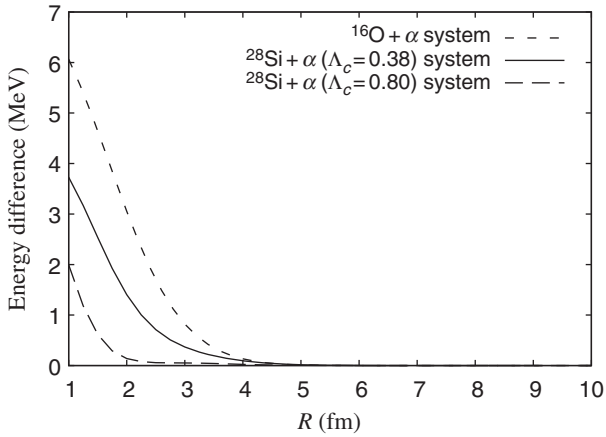

Fig. 16. The energy difference between the cases of the optimized λ_α and the fixed $\lambda_\alpha = 0$ for the $^{16}\mathrm{O} + \alpha$, $^{28}\mathrm{Si} + \alpha$ ($\Lambda_c = 0.38$), and $^{28}\mathrm{Si} + \alpha$ ($\Lambda_c = 0.80$) systems.

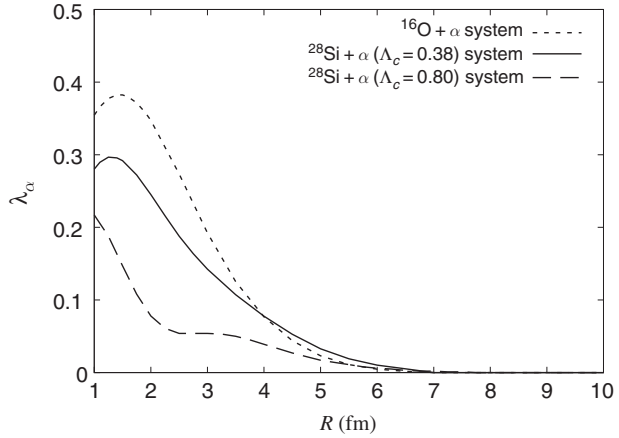

Fig. 17. The α-cluster breaking parameter λ_α optimized to minimize the energies of the $^{16}\mathrm{O} + \alpha$, $^{28}\mathrm{Si} + \alpha$ ($\Lambda_c = 0.38$), and $^{28}\mathrm{Si} + \alpha$ ($\Lambda_c = 0.80$) systems.

is opposite to this expectation. The reason is understood by the Pauli blocking effect from the ^{28}Si core as follows. In general, in the α-cluster breaking mechanism at the nuclear surface, four nucleons in the broken α cluster favor occupying the ls-favored orbits to gain the spin–orbit potential from the core rather than forming the ideal $(0s)^4$ α-cluster. However, in the $^{28}\mathrm{Si} + \alpha$ system, the ls-favored $0d_{5/2}$ orbits are occupied by nucleons in the ^{28}Si core, which block the α-cluster breaking. The $0d_{5/2}$ orbits are fully blocked in the jj-coupling limit $\Lambda_c = 1$ for the sub-shell $0d_{5/2}$-closed ^{28}Si core. Even though the ^{28}Si core in the ^{28}Si+α system is not in this limit, it has a finite Λ_c and partially blocks the $0d_{5/2}$ orbits. This picture can describe the suppression of the α-cluster breaking at the surface of the ^{28}Si core compared with that of the ^{16}O core where $0d_{5/2}$ orbits are empty, and also the larger suppression for the spherical-type ($\Lambda_c = 0.80$) ^{28}Si than that for the oblate-type ($\Lambda_c = 0.38$) ^{28}Si core.

5. Conclusion

We investigated the α-cluster excited states in ^{32}S. We proposed an extended model of the ^{28}Si+α cluster model by taking into account the ^{28}Si core deformation and rotation as well as the α-cluster

breaking. The ^{28}Si core is described by the extended 7α-cluster model with the cluster breaking due to the spin–orbit interaction.

Applying the extended ^{28}Si+α cluster model, we performed the GCM calculation and obtain the α-cluster excited states near the ^{28}Si+α threshold energy. These states construct the rotational band up to the 6^+ state with the rotational constant $k = 140$–150 keV. We cannot quantitatively predict the bandhead energy because of the ambiguity of the interaction parameters. The α-cluster excited band obtained in the present work may correspond to one of the experimentally reported bands [53,54]. The calculated rotational constant agrees reasonably with the value of the experimental band reported in Ref. [53]. Although the fragmentation of the α-cluster excited states was observed in the experiment of Ref. [53], no fragmentation is found in the present calculation, maybe because of the insufficient model space.

From the point of view of the strong coupling picture, we discussed the ^{28}Si core deformation and rotation effects as well as the α-cluster breaking effects in the α-cluster excited states. It is found that the rotation of the oblately deformed ^{28}Si core significantly reduces the excitation energies of the α-cluster excited states, whereas the α-cluster breaking gives only a minor effect. We also analyzed the feature of the α-cluster excited band from the weak coupling picture using the frozen core $^{28}\mathrm{Si}(0^+_{\mathrm{g.s.}}) + \alpha$ wave functions. The α-cluster excited states are found to have dominant $^{28}\mathrm{Si}(0^+_{\mathrm{g.s.}}) + \alpha$ components. The dimensionless reduced α widths estimated by the $^{28}\mathrm{Si}(0^+_{\mathrm{g.s.}}) + \alpha$ components are significantly large as $\theta^2_\alpha(a) = 0.26$–$0.32$ at $a = 6$ fm. We evaluated the partial α-decay widths from the calculated values of $\theta^2_\alpha(a)$. We also compared the result of the frozen core GCM calculation with that of the full GCM calculation, and found that the rotational excitation from $^{28}\mathrm{Si}(0^+_{\mathrm{g.s.}})$ plays a role in stabilizing the α-cluster excited states.

The present model is the extended ^{28}Si+α cluster model, in which cluster breaking due to the spin–orbit interaction and also the rotation of the deformed core are taken into account. The cluster breaking effect of the ^{28}Si core part gives a large energy reduction (18 MeV) of the isolate ^{28}Si from the 7α-cluster model without the cluster breaking. This is an advantage over conventional cluster models using the Brink–Bloch α-cluster model. Moreover, the rotation effect of the deformed core in ^{32}S gives about a 5 MeV reduction of the α-cluster band energy from that obtained with the fixed core orientation. This indicates the importance of the angular momentum projection of the subsystem in the α-cluster excited states having the deformed core.

Acknowledgements

This work was supported by JSPS KAKENHI Grant Number 26400270. The numerical calculations were carried out on the SR16000 at YITP in Kyoto University.

References

[1] K. Ikeda, H. Horiuchi, and S. Saito, Prog. Theor. Phys. Suppl. **68**, 1 (1980).
[2] S. Ohkubo, M. Fujiwara, and P. E. Hodgson, Prog. Theor. Phys. Suppl. **132**, 1 (1998).
[3] W. von Oertzen, M. Freer, and Y. Kanada-En'yo, Phys. Rep. **432**, 43 (2006).
[4] M. Freer, Rep. Prog. Phys. **70**, 2149 (2007).
[5] Y. Kanada-En'yo and H. Horiuchi, Prog. Theor. Phys. Suppl. **142**, 205 (2001).
[6] Y. Kanada-En'yo, M. Kimura, and H. Horiuchi, C. R. Physique **4**, 497 (2003).
[7] Y. Kanada-En'yo, M. Kimura, and A. Ono, Prog. Theor. Exp. Phys. **2012**, 01A202 (2012).
[8] H. Horiuchi, K. Ikeda, and K. Katō, Prog. Theor. Phys. Suppl. **192**, 1 (2012).
[9] W. Scholz, P. Neogy, K. Bethge, and R. Middleton, Phys. Rev. C **6**, 893 (1972).
[10] M. Gai, M. Ruscev, A. C. Hayes, J. F. Ennis, R. Keddy, E. C. Schloemer, S. M. Sterbenz, and D. A. Bromley, Phys. Rev. Lett. **50**, 239 (1983).

[11] P. Descouvemont and D. Baye, Phys. Rev. C **31**, 2274 (1985).
[12] M. Gai, R. Keddy, D. A. Bromley, J. W. Olness, and E. K. Warburton, Phys. Rev. C **36**, 1256 (1987).
[13] P. Descouvemont, Phys. Rev. C **38**, 2397 (1988).
[14] M. Freer et al., Phys. Rev. Lett. **82**, 1383 (1999).
[15] M. Freer et al., Phys. Rev. C **63**, 034301 (2001).
[16] G. V. Rogachev et al., Phys. Rev. C **64**, 051302 (2001).
[17] N. Curtis, D. D. Caussyn, C. Chandler, M. W. Cooper, N. R. Fletcher, R. W. Laird, and J. Pavan, Phys. Rev. C **66**, 024315 (2002).
[18] N. Soic et al., Phys. Rev. C **68**, 014321 (2003).
[19] M. Ito, K. Kato, and K. Ikeda, Phys. Lett. B **588**, 43 (2004).
[20] N. Curtis, N. I. Ashwood, N. M. Clarke, M. Freer, C. J. Metelko, N. Soić, W. N. Catford, D. Mahboub, S. Pain, and D. C. Weisser, Phys. Rev. C **70**, 014305 (2004).
[21] N. I. Ashwood et al., J. Phys. G **32**, 463 (2006).
[22] M. Kimura, Phys. Rev. C **75**, 034312 (2007).
[23] N. Furutachi, S. Oryu, M. Kimura, A. Dote, and Y. Kanada-En'yo, Prog. Theor. Phys. **119**, 403 (2008).
[24] C. Fu et al., Phys. Rev. C **77**, 064314 (2008).
[25] E. D. Johnson et al., Eur. Phys. J. A **42**, 135 (2009).
[26] W. von Oertzen et al., Eur. Phys. J. A **43**, 17 (2010).
[27] T. Suhara and Y. Kanada-En'yo, Phys. Rev. C **82**, 044301 (2010).
[28] H. Horiuchi and K. Ikeda, Prog. Theor. Phys. **40**, 277 (1968).
[29] J. Hiura, Y. Abe, S. Saito, and O. Endo, Prog. Theor. Phys. **42**, 555 (1969).
[30] W. Sünkel and K. Wildermuth, Phys. Lett. B **41**, 439 (1972).
[31] F. Nemoto and H. Bandō, Prog. Theor. Phys. **47**, 1210 (1972).
[32] T. Matsuse, M. Kamimura, and Y. Fukushima, Prog. Theor. Phys. **49**, 1765 (1973).
[33] F. Tanabe and F. Nemoto, Prog. Theor. Phys. **51**, 2009 (1974).
[34] Y. Suzuki, Prog. Theor. Phys. **55**, 1751 (1976).
[35] M. Libert-Heinemann, D. Baye, and P.-H. Heenen, Nucl. Phys. A **339**, 429 (1980).
[36] F. Michel, G. Reidemeister, and S. Ohkubo, Phys. Rev. Lett. **57**, 1215 (1986).
[37] F. Michel, G. Reidemeister, and S. Ohkubo, Phys. Rev. C **37**, 292 (1988).
[38] T. Wada and H. Horiuchi, Phys. Rev. C **38**, 2063 (1988).
[39] S. Ohkubo, Phys. Rev. C **38**, 2377 (1988).
[40] S. Ohkubo and K. Umehara, Prog. Theor. Phys. **80**, 598 (1988).
[41] A. C. Merchant, K. F. Pal, and P. E. Hodgson, J. of Phys. G **15**, 601 (1989).
[42] G. Reidemeister, S. Ohkubo, and F. Michel, Phys. Rev. C **41**, 63 (1990).
[43] T. Yamaya, S. Oh-ami, O. Satoh, M. Fujiwara, S. Hatori, T. Itahashi, K. Katori, S. Kato, M. Tosaki, and S. Ohkubo, Phys. Rev. C **41**, 2421 (1990).
[44] T. Yamaya, S. Oh-ami, M. Fujiwara, T. Itahashi, K. Katori, M. Tosaki, S. Kato, S. Hatori, and S. Ohkubo, Phys. Rev. C **42**, 1935 (1990).
[45] T. Yamaya, M. Saitoh, M. Fujiwara, T. Itahashi, K. Katori, T. Suehiro, S. Kato, S. Hatori, and S. Ohkubo, Phys. Lett. B **306**, 1 (1993).
[46] T. Yamaya, S. Ohkubo, S. Okabe, and M. Fujiwara, Phys. Rev. C **47**, 2389 (1993).
[47] T. Sakuda and S. Ohkubo, Phys. Rev. C **49**, 149 (1994).
[48] T. Yamaya, K. Ishigaki, H. Ishiyama, T. Suehiro, S. Kato, M. Fujiwara, K. Katori, M. H. Tanaka, S. Kubono, V. Guimaraes, and S. Ohkubo, Phys. Rev. C **53**, 131 (1996).
[49] T. Yamaya, K. Katori, M. Fujiwara, S. Kato, and S. Ohkubo, Prog. Theor. Phys. Suppl. **132**, 73 (1998).
[50] T. Sakuda and S. Ohkubo, Prog. Theor. Phys. Suppl. **132**, 103 (1998).
[51] M. Kimura and H. Horiuchi, Nucl. Phys. A **767**, 58 (2006).
[52] T. Tanabe, M. Yasue, K. Sato, K. Ogino, Y. Kadota, Y. Taniguchi, K. Obori, K. Makino, and M. Tochi, Phys. Rev. C **24**, 2556 (1981).
[53] T. Lönnroth, M. Norrby, V. Z. Goldberg, G. V. Rogachev, M. S. Golovkov, K.-M. Källman, M. Lattuada, S. V. Perov, S. Romano, B. B. Skorodumov, G. P. Tiourin, W. H. Trzaska, A. Tumino, and A. N. Vorontsov, Eur. Phys. J. A **46**, 5 (2010).
[54] M. Itoh, S. Kishi, H. Sakaguchi, H. Akimune, M. Fujiwara, U. Garg, K. Hara, H. Hashimoto, J. Hoffman, T. Kawabata, K. Kawase, T. Murakami, K. Nakanishi, B. K. Nayak, S. Terashima, M. Uchida, Y. Yasuda, and M. Yosoi, Phys. Rev. C **88**, 064313 (2013).
[55] D. M. Brink, H. Friedrich, A. Weiguny, and C. W. Wong, Phys. Lett. B **33**, 143 (1970).

[56] J. Zhang, W. D. M. Rae, and A. C. Merchant, Nucl. Phys. A **575**, 61 (1994).
[57] W. Bauhoff, H. Schultheis, and R. Schultheis, Phys. Rev. C **26**, 1725 (1982).
[58] F. Nemoto, Y. Yamamoto, H. Horiuchi, and Y. Suzuki, Prog. Theor. Phys. **54**, 104 (1975).
[59] N. Itagaki, J. Cseh, and M. P oszajczak, Phys. Rev. C **83**, 014302 (2011).
[60] Y. Kanada-En'yo, Phys. Rev. C **71**, 014303 (2005).
[61] Y. Taniguchi, M. Kimura, Y. Kanada-En'yo, and H. Horiuchi, Phys. Rev. C **76**, 044317 (2007).
[62] Y. Taniguchi, Y. Kanada-En'yo, and M. Kimura, Phys. Rev. C **80**, 044316 (2009).
[63] D. M. Brink, in Proceedings of the International School of Physics Enrico Fermi Course XXXVI, ed. C. Bloch (Academic, New York, 1966), p. 247
[64] T. Suhara, N. Itagaki, J. Cseh, and M. Płoszajczak, Phys. Rev. C **87**, 054334 (2013).
[65] D. L. Hill and J. A. Wheeler, Phys. Rev. **89**, 1102 (1953).
[66] J. J. Griffin, and J. A. Wheeler, Phys. Rev. **108**, 311 (1957).
[67] A. B. Volkov, Nucl. Phys. **74**, 33 (1965).
[68] N. Yamaguchi, T. Kasahara, S. Nagata, and Y. Akaishi, Prog. Theor. Phys. **62**, 1018 (1979).
[69] Y. Kanada-En'yo, T. Suhara, and Y. Taniguchi, Prog. Theor. Exp. Phys. **7**, 073D02 (2014).